JACS
JOURNAL OF THE AMERICAN CHEMICAL SOCIETY

ARTICLE

pubs.acs.org/JACS

Layered Hydrazinium Titanate: Advanced Reductive Adsorbent and Chemical Toolkit for Design of Titanium Dioxide Nanomaterials

Sergey N. Britvin,*[,†,‡] Andriy Lotnyk,[§] Lorenz Kienle,[§] Sergey V. Krivovichev,[†,‡] and Wulf Depmeier[∥]

[†]Department of Crystallography, Geological Faculty, St. Petersburg State University, Universitetskaya Nab. 7/9, 199034 St. Petersburg, Russia

[‡]Nanomaterials Research Center, Kola Science Center, Russian Academy of Sciences, 184200 Apatity, Murmansk Reg., Russia

[§]Institute for Material Science, Synthesis and Real Structure, University Kiel, Kaiserstrasse 2, 24143 Kiel, Germany

[∥]Institute for Geosciences, University Kiel, Olshausenstrasse 40, 24118 Kiel, Germany

Supporting Information

ABSTRACT: LHT-9, a layered hydrazinium titanate with an interlayer spacing of ~9 Å, is a new nanohybrid compound combining the redox functionality of hydrazine, the ion-exchange properties of layered titanate, the large surface area of quasi-two-dimensional crystallites, surface Brønsted acidity, and the occurrence of surface titanyl bonds. LHT-9, ideally formulated as $(N_2H_5)_{1/2}Ti_{1.87}O_4$, relates to a family of lepidocrocite-type titanates. It possesses a high uptake capacity of ~50 elements of the periodic table. Irreversibility of reductive adsorption allows LHT-9 to be used for cumulative extraction of reducible moieties (noble metals, chromate, mercury, etc.) from industrial solutions and wastewaters. Unlike sodium titanates that do not tolerate an acidic environment, LHT-9 is capable of uptake of transition metals and lanthanides at pH > 3. Adsorption products loaded with the desired elements retain their layered structures and can be used as precursors for tailored titanium dioxide nanomaterials. In this respect, the uptake of metal ions by LHT-9 can be considered as a method complementary to electrostatic self-assembly deposition (ESD) and layer-by-layer self-assembly (LBL) techniques. LHT-9 is readily synthesized in one step by a mild fluoride route involving hydrazine-induced hydrolysis of hexafluorotitanic acid under near-ambient conditions.

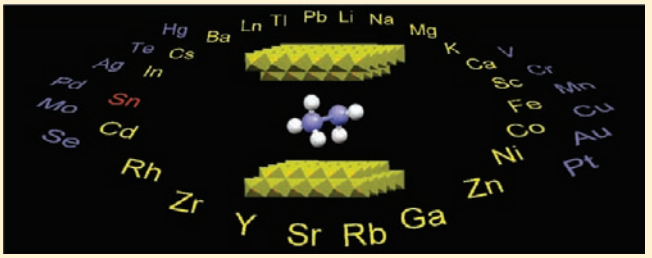

1. INTRODUCTION

The chemistry of nanocrystalline layered titanates represents an expanding area of materials science where the majority of research efforts are focused on catalytic activity and ion-exchange properties of titanate nanomaterials.[1] The capability of layered titanates to accommodate guest species between the layers opens a way for the construction of hybrid TiO_2-based compounds.[2] Herein we report on the crystal structure, properties, and application potential of a new nanohybrid compound, namely, layered hydrazinium titanate $(N_2H_5)_{1/2}Ti_{1.87}O_4$, which hereinafter is called LHT-9 because of its interlayer *d* spacing of ~9 Å. LHT-9 is related to a family of lepidocrocite-type layered titanates[3] with hydrazinium ion ($N_2H_5^+$) as principal constituent. Its parent compound hydrazine (N_2H_4) is a vital intermediate in synthetic chemistry, with applications ranging from fuel technology to organic chemistry[4] and the electronics industry.[5] It is known, however, that both hydrazine and its hydrate are toxic liquids that are sensitive to oxidation and catalytic decomposition.[4] Overcoming these drawbacks is still a challenging task in regard to the use of hydrazine in civil engineering applications, such as the introduction of direct hydrazine fuel cells (DHFCs) for public vehicles.[6] LHT-9 can be considered as a stable solid source of carrier-bound hydrazine in those applications where the usage of free hydrazine would be desirable but is restricted for safety reasons. LHT-9 is polyfunctional adsorbent exhibiting high uptake capacity of ~50 elements of the Periodic Table (Figure 1). The versatility of its adsorption behavior is a consequence of several factors: its redox properties inherited from the parent hydrazine, its ion-exchange properties resulting from the layered titanate structure, and the large surface area of quasi-two-dimensional (quasi-2D) nanocrystals. Surface acidity due to Brønsted acid sites and the occurrence of surface titanyl groups are additional factors that likely contribute to the adsorption activity of LHT-9. To the best of our knowledge, LHT-9 is the sole adsorbent simultaneously possessing reductive and ion-exchange properties. It can be used for cumulative extraction of noble metals (Rh, Pd, Pt, Au) from their solutions. Reductive adsorption can be exploited for removal of environmental pollutants (e.g., chromate or mercury) from industrial wastewaters. Unlike sodium titanates that are stable only in alkaline solutions,[1a] LHT-9 can tolerate acidic environments. The latter property allows nonhydrolytic uptake of transition metals and lanthanides at pH >3, yielding metal-loaded adsorption

Received: March 6, 2011
Published: May 25, 2011

dx.doi.org/10.1021/ja202053q | J. Am. Chem. Soc. 2011, 133, 9516–9525

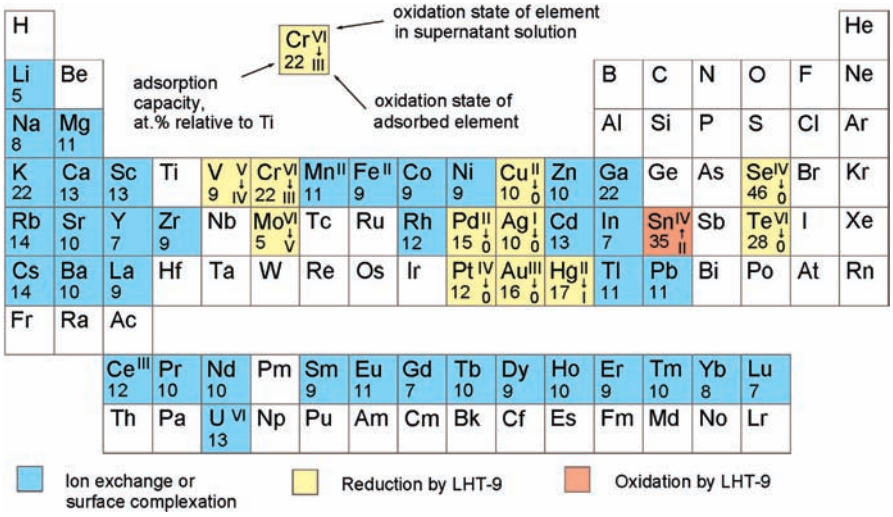

Figure 1. The periodic table. Highlighted are the elements that can be adsorbed by nanocrystalline LHT-9 in aqueous solutions. Depending on the nature of each element, different adsorption mechanisms can be proposed. The adsorption capacity of each element is given in atom % relative to Ti.

products that retain their layered structure. Such behavior opens a way for the construction of tailored titanium dioxide nanomaterials. In this respect, the use of LHT-9 can be considered as a preparative technique that is complementary to the electrostatic self-assembly deposition (ESD)[7] and layer-by-layer self-assembly (LBL)[8] methods conventionally employed for the preparation of metal-doped titanates. LHT-9 can be synthesized in two ways: (1) multistep solid-state synthesis and (2) a new "chimie douce" route involving alkali-induced hydrolysis of hexafluorotitanic acid (H_2TiF_6) under near-ambient conditions.[9,10] The latter method can be readily extended to other nanocrystalline titanates, as exemplified by the one-pot preparation of $Cs_{0.7}Ti_{1.83}O_4 \cdot 0.5H_2O$.

2. EXPERIMENTAL SECTION

2.1. Materials. Reagent grade H_2TiF_6 (60 wt % solution in water), hydrazine hydrate (~65% N_2H_4), CsOH (50 wt % aqueous solution), HCl (35 wt %), Cs_2CO_3, K_2CO_3, H_6TeO_6, $KMnO_4$, $AgNO_3$, RbCl, $HAuCl_4$, and absolute ethanol were obtained from Sigma-Aldrich, and anatase-type TiO_2 was purchased from Riedel-de-Haen. $AgMnO_4$ was prepared by exchange between $KMnO_4$ and $AgNO_3$ with subsequent recrystallization. Deionized water (18.2 MΩ cm^2) was used in all syntheses.

2.2. Synthesis. All of the syntheses were carried out under an air atmosphere except for the reduction of H_6TeO_6 by LHT-9, which was performed under a nitrogen atmosphere to avoid oxidation of the reduction product.

*2.2.1. Nanocrystalline LHT-9 (**1**).* The synthesis of **1** followed the fluoride route recently reported for the preparation of nanocrystalline niobates, tantalates, and germanates.[9] The details of the synthesis will be reported elsewhere.[10] Chemical composition [wt %, as determined by thermogravimetric analysis (TGA) with synchronous FTIR monitoring of evolved gases]: N_2H_4, 7.9; TiO_2, 71.9; H_2O, 20.3. This corresponds to a N_2H_4/Ti molar ratio of 0.27.

2.2.2. $Cs_{0.7}Ti_{1.83}O_4 \cdot 0.5H_2O$. H_2TiF_6 (0.3 M, 20 mL) was stirred with 20 mL of 50 wt % CsOH, after which the reaction mixture was boiled for 1 h. The obtained voluminous gel-like precipitate was thoroughly washed with an excess of water, filtered off, and dried overnight at 60 °C. Inductively coupled plasma (ICP) analysis gave a Cs/Ti atomic ratio of 0.38. The XRD pattern (Figure S1 in the Supporting Information) is consistent with that of lepidocrocite-type $Cs_{0.48}H_{0.22}(Ti_{1.825}O_4)(H_2O)_{0.5}$.[11a] Least-squares refinement of the unit cell parameters of $Cs_{0.7}Ti_{1.83}O_4 \cdot 0.5H_2O$ (orthorhombic, space group *Immm*) gave a = 3.799(1) Å, b = 17.710(4) Å, and c = 2.974(3) Å, in accordance with the lepidocrocite-type structure.

2.2.3. $Cs_{0.6}Ti_{1.8}O_4$, $H_{0.6}Ti_{1.8}O_4 \cdot nH_2O$, and $K_2Ti_2O_5$. These were synthesized by conventional solid-state methods.[11,12]

*2.2.4. Bulk LHT-9 (**2**).* $H_{0.6}Ti_{1.8}O_4 \cdot nH_2O$ (5 g) was treated with an excess of an aqueous solution of hydrazine (250 mL of hydrazine hydrate diluted with 250 mL of water) under continuous stirring for 12 h, thoroughly washed with an excess of water (five cycles of decantation), filtered off on filter paper, and dried in air at 60 °C overnight. Chemical composition (wt % by TGA with synchronous FTIR monitoring of evolved gases): N_2H_4, 8.6; TiO_2, 72.2; H_2O, 19.2. This corresponds to a N_2H_4/Ti molar ratio of 0.30.

2.2.5. $Rb_{1/4}(N_2H_5)_{1/4}Ti_{1.87}O_4 \cdot nH_2O$. Finely ground **1** (1 g) was suspended in 10 mL of water; 500 mg of RbCl was dissolved in 40 mL of H_2O (solution pH = 4.7) and then added to the suspension of **1**. After the suspension was stirred for 1 h, it was washed three times with an excess of water, filtered off, and air-dried overnight at 60 °C. The chemical composition [wt % as determined by energy-dispersive X-ray spectroscopy (EDX) for Rb, Cl, and Ti and TGA + FTIR for N_2H_4 and H_2O]: Rb_2O, 11.7; N_2H_4, 3.8; TiO_2, 69.6; H_2O, 14.9; Cl, below the detection limit. This corresponds to the formulation $Rb_{0.27}(N_2H_5)_{0.26}Ti_{1.87}O_4 \cdot 1.65H_2O$.

2.2.6. Tellurium/Layered Titania Nanocomposite. Finely ground **1** (3 g) was suspended in 100 mL of a 2 wt % solution of H_6TeO_6 in a glass flask under a nitrogen atmosphere. The suspension was heated to 50−60 °C with continuous stirring until the beginning of the reduction reaction (darkening of the LHT-9 powder with simultaneous effervescence of gaseous nitrogen) and then stirred for ~15 min to complete the reaction. After the reaction mixture was cooled, a black precipitate of the nanocomposite was gently separated from a thin, silvery layer of elemental Te (the latter was partially formed as a byproduct of the reaction), washed three times with an excess of absolute ethanol, and dried by slight heating under pumping. The nanocomposite could be stored infinitely under an inert atmosphere, but in air it was completely oxidized within 8−10 h.

2.3. Characterization. *Transmission Electron Microscopy.* Bright-field high-resolution transmission electron microscopy (HRTEM) and high-angle annular dark-field (HAADF) images for **1** were recorded with a Tecnai G^2 FEGTEM microscope operated at 300 kV. The samples were

dx.doi.org/10.1021/ja202053q | J. Am. Chem. Soc. 2011, 133, 9516–9525

prepared by dropping aqueous or alcohol suspensions of the titanates on carbon-supported copper grids followed by evaporation under ambient conditions.

Chemical Composition. The chemical compositions of **1** and **2** and the products of thermal decomposition of **1** were determined by TGA (heating to 1000 °C) with synchronous FTIR monitoring of evolved gases. FTIR traces of the gases were integrated in absorption windows of 980−900 cm^{-1} for NH_3 and 1570−1490 cm^{-1} for H_2O. The residues of thermal decomposition of **1** and **2** were both found to be titanium dioxide [mixtures of anatase and rutile, as determined by X-ray diffraction (XRD)]. Atomic ratios of the elements in the adsorption products (Figure 1) were determined by EDX (CamScan 4 scanning electron microscope with a LINK AN10000 EDX detector). For that purpose, fine powders of titanates were pressed into dense pellets with smooth surfaces using a 10 ton hydraulic press, glued onto conductive tape, vacuum-coated with a carbon film, and used for EDX analysis. Atomic adsorption and ICP analyses (for products of ion exchange with Li, Cs, Ba, Ce, and La) were conducted at the laboratories of Mekhanobr Engineering Ltd. (St. Petersburg, Russia).

X-ray Diffraction. Powder XRD patterns of nanocrystalline titanates were recorded on a STOE IPDS II image-plate diffractometer (Mo Kα, 40 kV, 50 mA, 200 mm detector-to-sample distance, 60 min exposure time per sample). Further processing of image-plate XRD data (radial averaging, background subtraction, and profile fitting) was carried out using the STOE X-Area 1.42 and WinXPOW 2.08 packages and Bruker OPUS 6.5 software. The crystal structure of **2** was solved from powder data (STOE Stadi P diffractometer, Cu Kα1) based on 27 reflections (SHELX-97).[13] Rietveld refinement of **2** was performed using the FULLPROF program suite.[14]

Thermal Analysis and FTIR. TGA and differential thermal analysis (DTA) curves for **1** were recorded on a Shimadzu TA-60 thermobalance (heating rate, 10 °C/min; nitrogen flow rate, 20 mL/min). FTIR spectra of the evolved gases were obtained with a Bruker Vertex 70 FTIR spectrophotometer equipped with an evolved-gas FTIR analyzer (fast nitrogen-cooled MCT detector) interfaced with a Netzsch TG 209 F1 thermobalance (heating rate, 10 °C/min; nitrogen flow rate, 20 mL/min). Solid-state FTIR spectra of titanates were recorded from standard KBr pellets using a Bruker Vertex 70 FTIR spectrophotometer at a resolution of 4 cm^{-1}.

X-ray Absorption Spectroscopy. Ti K-edge X-ray absorption fine structure (XAFS) spectra were recorded at beamline A1 of the DORIS III storage ring (DESY synchrotron facility, Hamburg, Germany) with a ring energy of 4.4 GeV and an average positron current of 110 mA. A double-crystal Si(311) monochromator installed at the beamline was detuned to 60% to eliminate higher-order harmonics. The spectra were recorded in transmission mode at room temperature from pellets made of titanates diluted with boron nitride. The energy scans were performed with steps of 0.2 eV in the X-ray absorption near-edge structure (XANES) region and 2 eV below and above the XANES region. Ti foil was used as the reference standard. Data processing was carried out using the IFEFFIT-Athena and FEFF-Artemis packages.[15]

3. RESULTS AND DISCUSSION

3.1. Fluoride Synthesis. Like recently described syntheses of nanocrystalline niobates, tantalates, and germanates by hydrolysis of the corresponding fluoro complexes,[9] the fluoride synthesis of **1** exploited the high stability of hexafluorotitanate ion (TiF_6^{2-}) against hydrolytic decomposition, as indicated by its hydrolysis constant (based on the reaction $TiF_6^{2-} + 3H_2O \rightarrow TiO(OH)_2\downarrow + 4H^+ + 6F^-$), which is on the order of 10^{-34}.[16] Alkali-induced hydrolysis of H_2TiF_6 leads to the formation of nanocrystalline titanates intercalated with a variety of cations, depending on the composition of the starting solution. Using hydrazine as the source of alkali yielded layered hydrazinium titanate. Using CsOH resulted in the one-pot synthesis of $Cs_{0.7}Ti_{1.83}O_4 \cdot 0.5H_2O$, the nanocrystalline analogue of the lepidocrocite-type titanate conventionally synthesized by multistep solid-state synthesis.[11] The fluoride synthesis of **1** gave white homogeneous powders of LHT-9 composed of heavily bent nanoleaves (Figure 2). The fluorine content in **1** was less than 0.2 wt % (as determined by a TEM EDX checkup), indicating complete hydrolysis of H_2TiF_6.

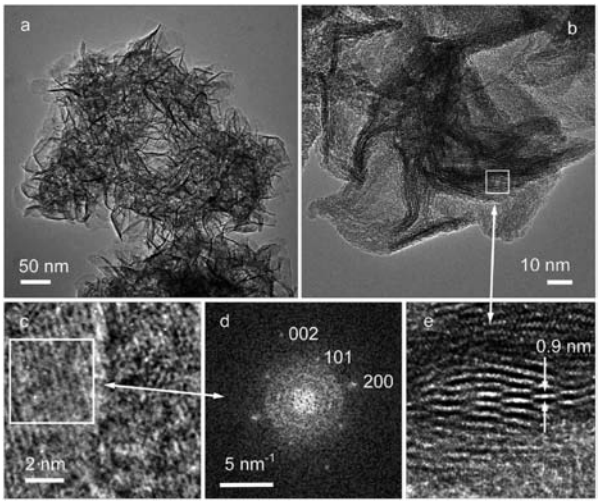

Figure 2. Bright-field HRTEM images of **1**. (a) General view of a flaky aggregate. (b) Heavily bent quasi-2D nanoleaves with thicknesses of 3−10 interlayer spacings. (c) Detail of the basal section of a nanoleaf. (d) FFT pattern corresponding to (c), showing the orthogonal in-plane lattice. (e) Detail of (b) showing numerous stacking faults. The observed lattice fringes correspond to an interlayer spacing of 0.9 nm.

3.2. Crystal Structure. The solution of the structure of **2** and subsequent Rietveld refinement (Figure S3 and Tables S4 and S5 in the Supporting Information) revealed orthorhombic symmetry (space group *Immm*) with the following lattice parameters: a = 3.7926(4) Å, b = 18.458(2) Å, c = 2.9774(2) Å, and V 208.43(5) Å ^{3}. LHT-9 displays analogy to a family of layered titanates with crystal structures derived from lepidocrocite, γ-FeO(OH).[3] In the structures of lepidocrocite-type titanates with body-centered (I) or base-centered (C) lattices, edge-facing stacking of infinite flat double sheets composed of TiO_6 octahedra results in the formation of interlayer "pseudochannels" having a relatively large diameter that are directed along the c axis, as shown in Figure 3. The occurrence of these pseudochannels may help explain a peculiarity of the intercalation behavior of lepidocrocite-type titanates, namely that when the latter are intercalated with large cations (K^+, Rb^+, Cs^+, NH_4^+, NMe_4^+), they unequivocally adopt C- or I-centered lattices.[3,11,17] This phenomenon can be explained by preferred tailoring of adjacent titanate sheets, which forces them to host large cations in the pseudochannels. In LHT-9, hydrazinium ions are stacked with the nitrogen−nitrogen bonds directed along the pseudochannels (Figure 3). It arguably appears that such linear linking (contrary to the zigzag one observed, e.g., in hydrazine-intercalated layered chalcogenides[5f]) is also forced by the influence of the host titanate pseudochannels.

The N−N bond length in **2** was found to be equal to 1.36(2) Å, which deviates by 6% from the N−N bond length of 1.45(2) Å in hydrazine and hydrazinium ions;[18] this discrepancy is the

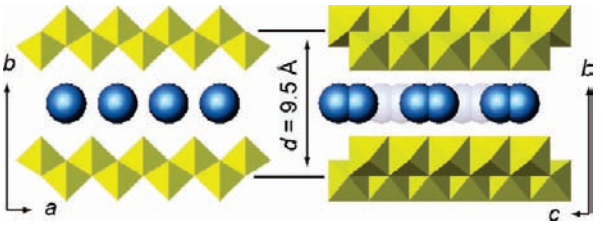

Figure 3. Crystal structure of LHT-9, with projections onto (right) (001) and (left) (100). Edge-faced stacking of corner-sharing TiO_6 octahedra (yellow) results in the formation of interlayer "pseudochannels" directed along the *c* axis. These pseudochannels are half-occupied by hydrazinium ions (blue spheres depict the front row and grayish spheres the back row) tailored in such a way that N−N bonds are directed along the pseudochannels. The relative sizes of the shown structural units are consistent with their actual size ratios.

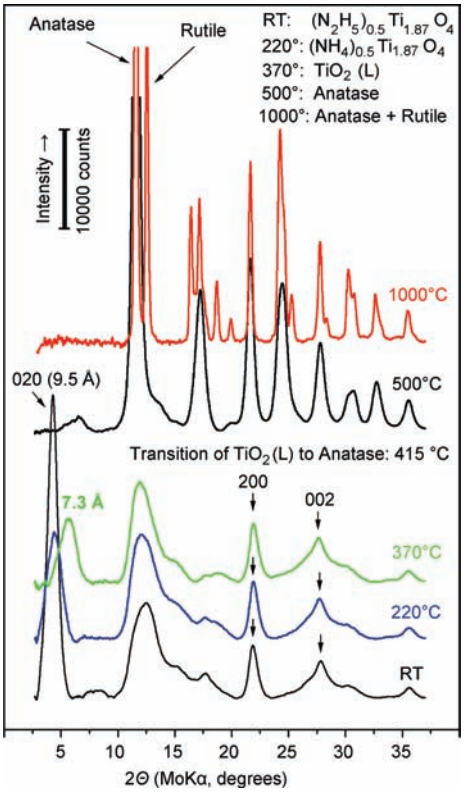

Figure 4. Powder XRD patterns of as-synthesized **1** at room temperature (RT) and of products formed by heating of **1** to various temperatures under a nitrogen flow.

result of experimental uncertainities during free Rietveld refinement of the position of the nitrogen atom. Direct structure solution of **1** (nanocrystalline LHT-9) was not possible because of the poor quality of its XRD pattern (Figure 4). The latter can be clarified by HRTEM observations (Figure 2): nanoleaves of **1** having thicknesses of 3−10 interlayer spacings are in fact quasi-2D nanosheets similar to the 2D titanate and niobate nanosheets prepared by exfoliation techniques.[19] Numerous stacking faults and bending of nanoleaves (Figure 2) are also unfavorable for coherent X-ray scattering; however, the lattice fringes observed in the HRTEM images of the nanoleaves correspond to an interlayer distance of ∼0.9 nm (Figure 2e). Fast Fourier

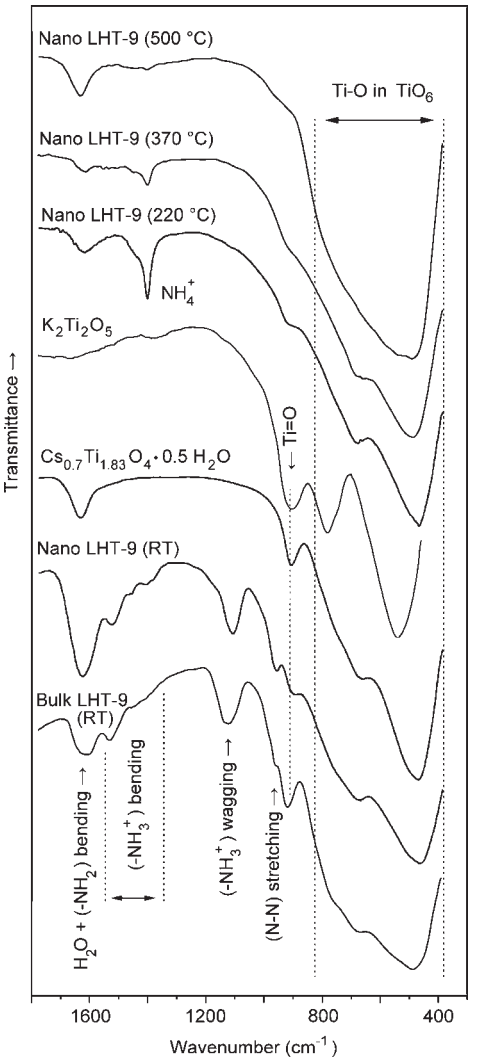

Figure 5. FTIR spectra of as-synthesized **1** and **2** at room temperature and of products formed by heating of **1** to various temperatures under a nitrogen atmosphere.

transform (FFT) patterns of the basal nanoleaf sections indicated that the latter possess an orthogonal in-plane lattice with translational periods of ∼0.3 and ∼0.4 nm (Figure 2c,d). These data are consistent with the unit cell dimensions of **2**, which were used as starting values for fitting of the XRD pattern of **1** (Figure S6 in the Supporting Information). Subsequent indexing and least-squares refinement based on 10 well-fitted reflections of **1** (Table S7 in the Supporting Information) gave an *I*-centered orthorhombic cell with the following refined parameters: a = 3.761(7) Å, b = 18.61(2) Å, and c = 2.953(4) Å. These data, along with FTIR evidence given below, led to the conclusion that **1** possesses a lepidocrocite-type structure.

3.3. Hydrazinium Ion and Chemical Formula. Hydrazine ($H_2N-NH_2 \equiv N_2H_4$) is a weak base ($pK_b = 6.0$)[20] that can be protonated to form singly charged ($H_2N-NH_3^+ \equiv N_2H_5^+$) or doubly charged ($^+H_3N-NH_3^+ \equiv N_2H_6^{2+}$) hydrazinium ions.[4] It has been shown that IR spectroscopy can provide information on the protonation state of hydrazine in its compounds.[21,22] The FTIR spectra of **1** and **2** (Figure 5) contain exactly the same series of absorption bands attributable to the bending (1526, 1464, 1408, 1386 cm^{-1}) and wagging (1107 cm^{-1}) vibrations of

dx.doi.org/10.1021/ja202053q | J. Am. Chem. Soc. 2011, 133, 9516–9525

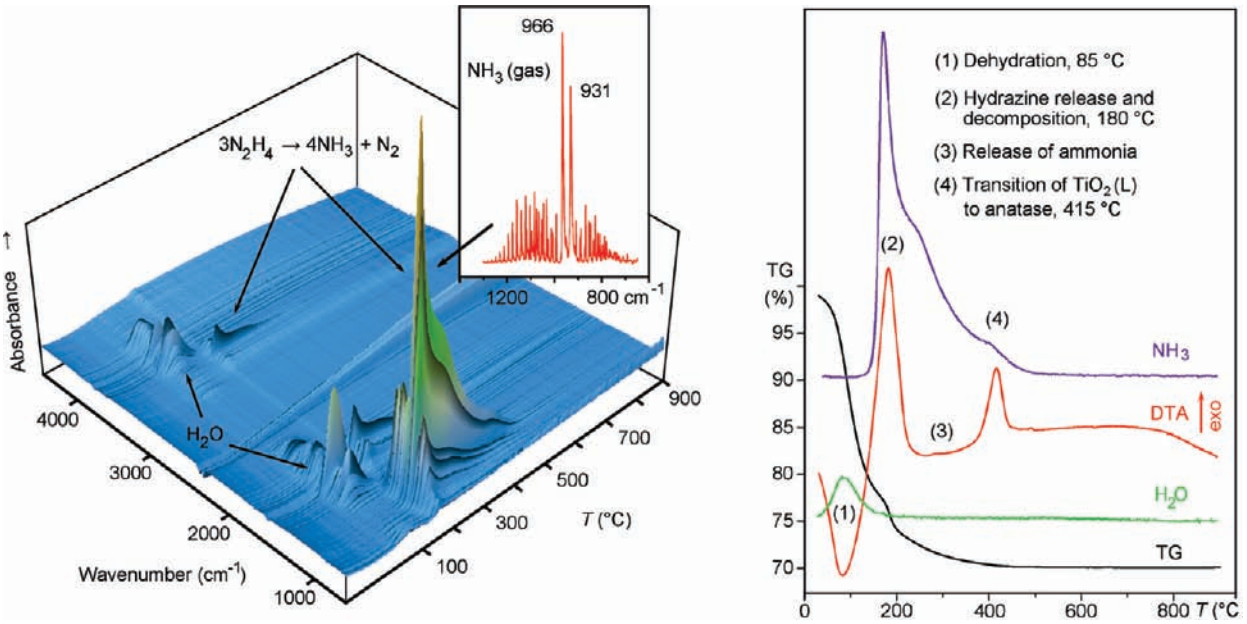

Figure 6. Thermal decomposition behavior of **1**. (left) 3D view of the evolved-gas FTIR spectrum of **1**; the inset shows the FTIR spectrum of ammonia vapor formed by decomposition of the released hydrazine. (right) TGA, DTA, and evolved H_2O and NH_3 gas curves of **1**.

the charged $-NH_3^+$ part of hydrazinium ion.[21] These findings confirm that (1) hydrazine in LHT-9 occurs in the charged protonated state rather than as the neutral hydrazine molecule and (2) the structural positions of the hydrazinium ions in the crystal structures of **1** and **2** are identical. However, $-NH_3^+$ may occur in both $N_2H_5^+$ and $N_2H_6^{2+}$ ions, raising ambiguity in the assignment of the hydrazinium charge. The latter can be resolved by the analysis of the band frequency related to the N−N stretching vibration, as its position in the IR spectra of hydrazine derivatives is sensitive to the local environment of nitrogen. In particular, this band occurs in the range 958−979 cm^{-1} in salts of $N_2H_5^+$ and 1024−1027 cm^{-1} in compounds of $N_2H_6^{2+}$.[22] The N−N stretching band in the spectrum of LHT-9 appears at 958 cm^{-1}, corresponding to singly charged $N_2H_5^+$. Intercalation of positively charged hydrazinium ions in the interlayer of LHT-9 implies that the host titanate sheets have to bear negative charge. It should be noted that full occupancy of the octahedral sites by Ti^{4+} in lepidocrocite-type titanates would result in zero charge for the titanate sheets. In the absence of low-charge octahedral cations (Li^+, Mg^{2+}, etc.) substituting for Ti^{4+} and in the absence of Ti^{3+} (which is known as a stronger reductant than hydrazine and would be unlikely to be formed from Ti^{4+} in the oxidizing atmosphere), negative charge can be achieved only by Ti vacancies in TiO_6 octahedra.[23] These considerations agree well with the chemical composition of **2** and the freely refined site occupancies for Ti and N in the structure of **2** (Table S5 in the Supporting Information), which lead to an empirical formula for **2** of $(N_2H_5)_{0.56}(Ti_{1.78}\square_{0.22})O_{3.84}$, where □ denotes a vacancy in a TiO_6 octahedron. In accordance with that, the chemical composition of **1** is explained well by the formula $(N_2H_5)_{0.5}$-$(Ti_{1.87}\square_{0.13})O_4$. Notably, the Rietveld refinement of the crystal structure of **2** did not reveal any extra moieties other than hydrazinium ions in the interlayer space of LHT-9: all of the electron density localized in the interlayer was correlated with the contents of hydrazine determined by TGA−FTIR. Because of its molecular geometry and hydronium-like ability to create strong hydrogen bonds,[4] the hydrazinium ion itself can maintain both charge balance and interlayer space filling of the layered titanate structure. Consequently, water cannot be considered as a required constituent of LHT-9. On the basis of the TGA−FTIR results and structure refinement, the general formula of LHT-9 can be expressed as $(N_2H_5)_x(Ti_{2-x/4}\square_{x/4})O_4$. However, because the syntheses of LHT-9 were carried out in an aqueous environment, the presence of a subordinate amount of molecular water in the interlayer cannot be ruled out.

3.4. Thermal Behavior and Evidence of TiO_2(L) Phase. The anhydrous state of LHT-9 is supported by thermal analysis of **1** (Figure 6), which indicated that water was totally released in one step with maximum rate at 85 °C. Dehydration was reversible and did not affect the interlayer spacing of **1**. Such behavior indicates that the adsorbed H_2O is weakly bound. Dehydration was followed by evolution and decomposition of hydrazine, which occurred between 150 and 220 °C with a maximum rate at 180 °C. It is known that self-decomposition of hydrazine may proceed in two ways: $N_2H_4 \rightarrow N_2 + 2H_2$ (scheme 1) or $3N_2H_4 \rightarrow 4NH_3 + N_2$ (scheme 2).[4] The first pathway typically requires catalytic activation (e.g., by Pt metal), while the second one is energetically favorable.[4] In the present case, strong absorption bands of NH_3 were observed in the FTIR spectra of the evolved gas, thus evidencing scheme 2. However, because the data depicted in Figure 6 were obtained from the sample heated in Pt crucible, we repeated the same experiment using a porcelain crucible in order to avoid the possibility of catalytic influence of Pt on hydrazine decomposition. The results of the two experiments were found to be essentially the same. Therefore, one can assume that Pt has just a negligible catalytic effect on the decomposition of hydrazine evolved from LHT-9. The release and decomposition of hydrazine was accompanied by exothermic peaks in the DTA diagrams, with an estimated molar reaction heat of 56 kJ/mol of $(N_2H_5)_{0.5}Ti_{1.87}O_4$. Visually, this process appeared as flash self-ignition of the substance to dull-red heat, but surprisingly, it did not lead to destruction of the layered

dx.doi.org/10.1021/ja202053q | J. Am. Chem. Soc. 2011, 133, 9516–9525

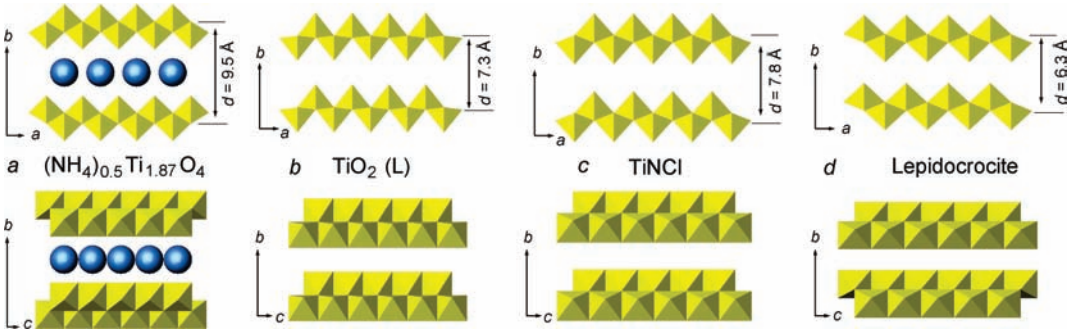

Figure 7. (a, b) Proposed structural models for layered titanates obtained by heating of **1** under a nitrogen flow: (a) layered ammonium titanate (220 °C); (b) layered lepidocrocite-type TiO_2(L) (370 °C). (c, d) Crystal structures of (c) TiNCl (space group *Pmnm*, cell setting $b > a > c$) and (d) lepidocrocite (space group *Cmcm*, cell setting $b > a > c$) are shown for comparison. The upper and lower rows are projections onto (001) and (100), respectively. Yellow octahedra, MO_6; blue balls, ammonium ions. The relative sizes of drawn structural units are consistent with their actual size ratios.

structure. Such behavior can occurs for kinetic reasons, namely, that hydrazine decomposition proceeds so rapidly that it does not result in immediate structural changes. It is interesting to note that the evolution of hydrazine from another layered hydrazinium compound, $N_4H_9Cu_7S_4$, is endothermic,[5f] so the strong exothermic effect observed for LHT-9 must be explained by chemical peculiarities of the latter, including a possible catalytic influence of the nanocrystalline titania matrix. Heating of **1** to 220 °C yielded a layered titanate with a basal spacing of 9.5 Å and undisplaced positions of the (200) and (002) reflections (see the XRD pattern in Figure 4), indicating that the lattice parameters of the substance retained essentially the same.

However, this titanate contains ammonium instead of hydrazinium in the role of charge-balancing cation, as confirmed by the single characteristic FTIR absorption band at 1400 cm^{-1} (Figure 5). It can be seen (see Figure S8 in the Supporting Information) that the effective ionic radius of ammonium ion is equal to the ionic radius of hydrazinium if the latter (as in the case of LHT-9) is laterally stacked in the interlayer space. This explains why the lattice parameters of hydrazinium and ammonium titanates are essentially the same. On the basis of the amount of ammonia evolved from **1** at this stage of thermal decomposition as well as charge-balance considerations, the chemical formula of ammonium titanate can be expressed as $(NH_4)_{0.5}Ti_{1.87}O_4$. The proposed model of its crystal structure is shown in Figure 7a. Its FTIR spectrum, however, contains a broad band at 1620 cm^{-1} attributable to bending vibrations of molecular H_2O. The origin of this (possibly readsorbed) water requires further studies. The layered ammonium titanate decomposes between 220 and ~350 °C with gradual evolution of ammonia, as traced by the shoulder on the NH_3 release curve (Figure 6). According to the FTIR spectrum (Figure 5) and TGA curve, the product of heating to 370 °C is titanium dioxide containing ~0.5 wt % NH_3 and possible traces of H_2O. The XRD data show that this substance retains a layered structure in which the basal spacing is shrunk to 7.3 Å while the positions of the (200) and (002) reflections remain unshifted (Figure 4). Its interlayer *d* spacing of 7.3 Å is intermediate between the values of 6.3 Å for lepidocrocite, γ-FeO(OH), and 7.8 Å for lepidocrocite-type TiNCl[24] and therefore, like those, is too narrow to host any interlayer moieties (i.e., NH_4^+ or H_2O) (Figure 7). On the basis of TGA–FTIR data on its chemical composition (confirming that this compound is titanium dioxide) and the value of its interlayer *d* spacing (which does not allow it to host interlayer

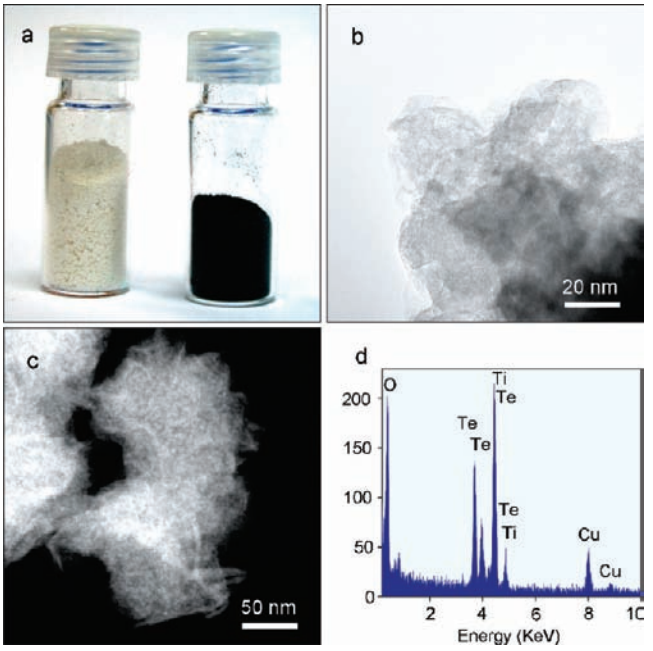

Figure 8. Tellurium/layered titania nanocomposite obtained by reduction of H_6TeO_6 on **1**. (a) (left) as-prepared powder of **1**; (right) product of reduction of H_6TeO_6. (b) Bright-field HRTEM and (c) HAADF (*Z*-contrast) image of the nanocomposite showing that the substance is homogeneous on the nanometer scale. (d) EDX spectrum taken from the area of (c).

moieties), one can suppose that heating of **1** to 370 °C under a nitrogen flow results in the formation of a new polymorph of titanium dioxide, which hereinafter is called TiO_2(L). The latter likely possesses a layered lepidocrocite-type structure with the lattice parameters $a = 3.74$ Å, $b = 7.3$ Å, and $c = 2.98$ Å. The best fit of the observed and calculated intensities of the XRD patterns was achieved assuming the TiNCl structure type,[24] which is based on space group *Pmnm* in the cell setting $b > a > c$, as accepted for lepidocrocite-type titanates. The proposed model for its crystal structure is shown in Figure 7b. TiO_2(L) was formed by decomposition of **1** in a narrow temperature range between ~370 and 400 °C. It was exothermically transformed into anatase at 415 °C (Figure 6). Further heating resulted in the gradual transformation of anatase into rutile, but the product of

dx.doi.org/10.1021/ja202053q | *J. Am. Chem. Soc.* 2011, 133, 9516–9525

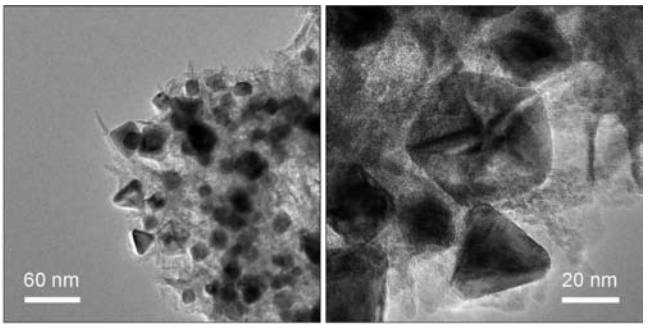

Figure 9. Bright-field HRTEM images of octahedral, cubic, and icosahedral palladium nanocrystals on nanocrystalline layered titania obtained by reduction of Na_2PdCl_4 by **1**.

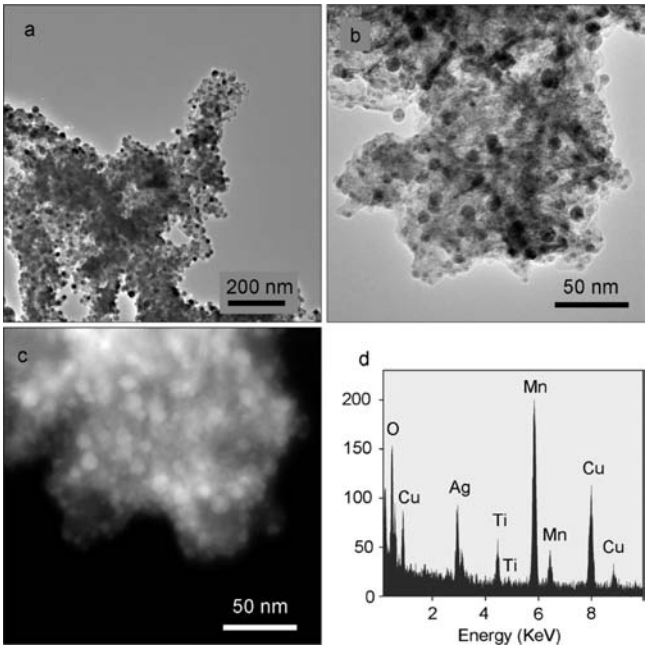

Figure 10. MnO_2/layered titania nanocomposite impregnated with Ag nanocrystals (light balls in the HAADF image) obtained by reductive adsorption of $AgMnO_4$ by **1**: (a, b) bright-field HRTEM images; (c) HAADF (*Z*-contrast) image; (d) EDX spectrum taken from the area of (c).

annealing to 1000 °C was still a mixture of anatase and rutile (Figure 4).

3.5. Redox Properties. LHT-9 is an effective reducing agent that has the redox properties of hydrazine superimposed onto the adsorption properties of the nanocrystalline titanate matrix, resulting in the phenomenon of reductive adsorption. As an example, the reaction of telluric acid (H_6TeO_6) with **1** (see section 2.2.6) yielded a black nanocomposite of Te with titania that was homogeneous on the nanometer scale (Figure 8) and retained a layered structure (Figure S9 in the Supporting Information). Palladium was readily reduced from a cold 2% solution of Na_2PdCl_4 with the formation of Pd nanocrystals (Figure 9). When the supernatant solution contained two elements that could be reduced, the latter could behave in diverse ways. Figure 10 shows silver nanocrystals precipitated on nanoleaves of the layered hydrous MnO_2/layered titania composite obtained by reduction of a 0.2 wt % $AgMnO_4$ solution by **1**. Depending on the concentration, temperature, and chemical

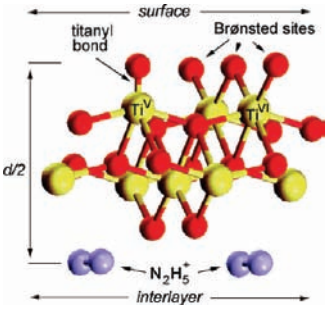

Figure 11. Suggested positions of the Brønsted acid sites and titanyl bonds at the surface of a titanate sheet in LHT-9.

nature of each element, reductive adsorption on LHT-9 was completed within a time between a few minutes and 1 h. LHT-9 can work as a reductive adsorbent at pH between 1 and 10. The uptake capacities and proposed reduction pathways are summarized in Figure 1. To the best of our knowledge, LHT-9 is likely the sole polyfunctional reductive adsorbent known to date. A typical reduction pathway can be illustrated by the fast (completed within 1−2 min) reduction of gold from a 0.2 M solution of $HAuCl_4$, represented by the scheme $4HAuCl_4 + 6(N_2H_5)_{0.5}Ti_{1.87}O_4 \rightarrow 4Au\downarrow + 6H_{0.5}Ti_{1.87}O_4 + 3N_2\uparrow + 16HCl$.

The latter reaction, which is accompanied by effervescence (nitrogen gas) and an abrupt change of color of the adsorption product (from initially white to green-black or violet-brown), can be used as sensitive test for residual hydrazine in LHT-9 and its reaction products. Because of the irreversibility of the majority of reduction reactions under the given redox conditions, LHT-9 can be used for cumulative extraction of reducible elements from their solutions. The sole ion that was found to be oxidized by LHT-9 is Sn^{2+}. Preliminary studies of the adsorption products indicated that Sn^{2+} is partially oxidized to Sn^{4+}; the detailed report will be published separately.

3.6. Ion Exchange and Protonation. LHT-9 exhibits high rates of ion-exchange and protonation reactions. Complete protonation of **1** in 1 M HCl was accomplished within 30 min. The protonated layered titanate showed no reaction with $HAuCl_4$, indicating the elimination of hydrazinium by acid treatment. The FTIR spectrum of acid-treated **1** showed no signs of hydrazinium and possessed the same absorption bands as the FTIR spectrum of bulk $H_{0.6}Ti_{1.8}O_4 \cdot nH_2O$ obtained by solid-state synthesis[11a] (Figure S10 in the Supporting Information). The powder XRD pattern of protonated **1** (Figure S11 in the Supporting Information) revealed that the substance still retained the layered structure. Ion-exchange reactions with **1** were typically complete within 30−60 min. Ion exchange may result in a change of interlayer distance in the reaction product, as illustrated by the expansion of the *d* spacing in $(N_2H_5)_{0.25}Rb_{0.25}Ti_{1.87}O_4 \cdot nH_2O$ from 9.5 to 10.2 Å (Figure S12 in the Supporting Information). The majority of exchange products, however, were found to contain hydrazinium, as they showed positive tests for hydrazine with $HAuCl_4$ and contained bands characteristic of hydrazinium in their FTIR spectra. The latter is exemplified by the FTIR spectrum of $(N_2H_5)_{0.25}Rb_{0.25}Ti_{1.87}O_4 \cdot nH_2O$ (Figure S13 in the Supporting Information). Incomplete ion exchange may be considered an advantage of LHT-9, since its reductive adsorption properties even under competitive ion exchange are retained. Moreover, this property

dx.doi.org/10.1021/ja202053q | *J. Am. Chem. Soc.* 2011, 133, 9516–9525

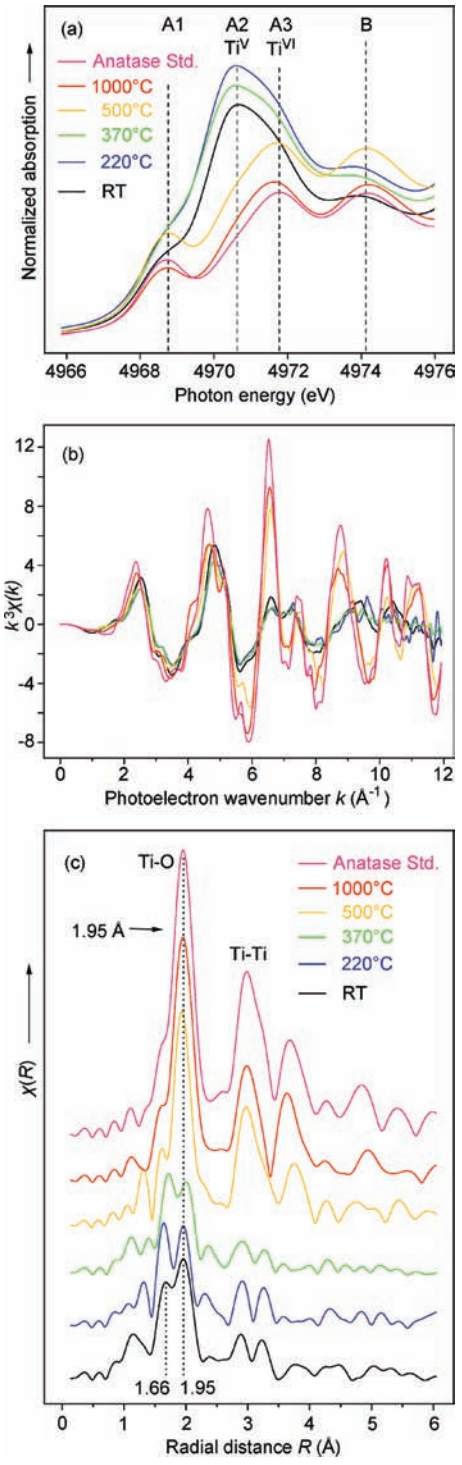

Figure 12. (a) XANES Ti pre-K-edge region, (b) k^3-weighted EXAFS oscillations, and (c) corresponding magnitudes of the phase-shift-corrected FTs of the radial distribution functions of **1** at room temperature (RT) and of the products formed by heating of **1** to various temperatures [$(NH_4)_{0.5}Ti_{1.87}O_4$ (220 °C); TiO_2(L) (370 °C); anatase (500 °C); anatase + rutile (1000 °C)]. The spectrum of an anatase standard is shown for comparison purposes.

allows the preparation of layered titanates with tailored functionality that contain desired exchanged ions and simultaneously possess reductive properties. Further chemical modification and/or thermal treatment of such intermediates can be used for the preparation of doped titanium dioxide nanomaterials.

3.7. Surface Acidity. It has been shown that protonated samples of lepidocrocite-type titanates $H_xTi_{2-4x}O_4 \cdot nH_2O$ behave as strong Brønsted acids.[2a] Brønsted acidity is likely caused by protonation of bridging Ti−O−Ti oxygen atoms located at loose corners of TiO_6 octahedra exposed at the surfaces of the titanate layers (Figure 11), similarly to Brønsted acid sites in exfoliated niobate, titanate, and tantalate nanosheets.[19,25] In quasi-2D nanoleaves of **1** (Figure 2a,b), a relative share of acidic sites exposed at the outer surfaces of the nanoleaves and therefore uncompensated by interlayer hydrazinium should be very large. Likely because of this phenomenon and despite the fact that **1** was synthesized in an alkaline environment (pH ≈ 8), aqueous suspensions of as-synthesized and air-dried **1** exhibited acidity (pH 6.2−6.4). This important property allows the hydrolysis of ions of transition metals and lanthanides in suspensions of **1** to be eliminated. Therefore, one can overcome one inherent drawback of sodium titanates: the limitation of the exchange of transition metals to ammine complexes under alkaline conditions.[1a] The direct adsorption of transition metals and lanthanides by **1** can be conducted at pH 3−7, yielding layered titanates loaded with the desired elements. Maximal loading was typically accomplished within ~30 min; the corresponding uptake capacities are given in Figure 1. Uptake of transition metals and lanthanides is a convenient route to doped layered TiO_2 nanomaterials because the reaction products do not contain undesired cationic pollutants, which are unavoidable when using titanates of alkali metals. In this respect, the sorption of metals by LHT-9 represents a preparative technique complementary to ESD[7] and LBL.[8] The latter methods are conventionally employed for the preparation of metal-doped layered TiO_2 nanomaterials, but both require the multistep synthesis of exfoliated titania precursors.[7,8] The exact mechanisms of sorption of transition metals and lanthanides by LHT-9, however, require further investigation. They can equally involve surface complexation as well as ion-exchange reactions.

3.8. Five-Coordinate Titanium and Titanyl Bonds. Since Farges et al.[26] demonstrated that the local coordination environment of titanium in oxide compounds can be determined from the fine structure of the Ti pre-K-edge region in XANES spectra, many groups have reported on the square-pyramidal coordination of Ti (labeled "Ti^V") in nanoparticles of anatase-type TiO_2.[27] Such fivefold coordination of Ti is revealed by the characteristic peak at 4970.5 eV (A2 in the notation of Farges et al.[26]), while the peak at 4971.5 eV (A3) is assigned to sixfold (octahedrally) coordinated titanium.[26] The existence of Ti^V, which may not occur in the crystal structure of anatase, is explained by local defects and truncation of TiO_6 octahedra at the surface of the nanoparticles.[27] In layered titanates, the A2 peak is dominant in the Ti pre-K-edge XANES region of $K_2Ti_2O_5$,[26] the latter being a classic example of a compound having square-pyramidal coordination of Ti^V.[28] The crystal structures of other layered titanates, both lepidocrocite-type ones[3,23] and those related to the $A_2Ti_nO_{2n+1}$ family (A denotes an alkali cation; $n = 3-5$)[29] do not contain Ti^V. However, their XANES spectra frequently show the A2 peak,[30] though its assignment to five-coordinate Ti is not always discussed.[31] Figure 12a depicts the Ti pre-K-edge XANES spectra of **1** and the products of its thermal transformations. The comparison +reveals that the A2 peak dominates in the spectra of **1** and its layered derivatives $(NH_4)_{0.5}Ti_{1.87}O_4$ and TiO_2(L).

dx.doi.org/10.1021/ja202053q | J. Am. Chem. Soc. 2011, 133, 9516–9525

The subsequent transition of TiO_2(L) to anatase (Figure 6) is accompanied by the disappearance of the A2 peak. Therefore, the XANES data provide substantial evidence of the existence of Ti^V in **1** and its layered derivatives. Further evidence is provided by the analysis of Ti K-edge EXAFS spectra, where, as in XANES, the products of the thermal transformations of **1** are clearly divided into two subgroups (Figure 12b,c). The Fourier transforms (FTs) of the EXAFS oscillations of anatase and anatase−rutile mixtures (produced by heating of **1** to 500 and 1000 °C, respectively) show a strong single peak attributed to a first shell of octahedrally coordinated titanium with a mean Ti−O distance of 1.95 Å.[26] In contrast, FTs of the EXAFS of LHT-9, $(NH_4)_{0.5}Ti_{1.87}O_4$, and TiO_2(L) display a remarkable feature: the peak attributed to a first coordination shell of Ti is split into a sharp doublet with Ti−O distances of 1.95 and 1.66 Å. The peak at 1.66 Å can undoubtedly be assigned to a short titanyl Ti═O bond characteristic of square-pyramidal coordination of titanium (Figure S14 in the Supporting Information).[28] Thus, both the XANES and EXAFS data concordantly indicate the presence of five-coordinate Ti in **1** and the products of its thermal decomposition. Attempts to simulate the EXAFS spectra of **1** using the FEFF−Artemis package[15] and the structural model of LHT-9 were unsuccessful, obviously because the latter (Figure 3 and Figure S14 in the Supporting Information) implies only six-coordinate Ti and does not permit the existence of Ti^V. The best fit was achieved assuming mixed coordination of titanium (∼70% Ti^{VI} and ∼30% Ti^V), with scattering paths for Ti^{VI} adopted from the structural model of LHT-9 and paths for Ti^V calculated from the structural model of $K_2Ti_2O_5$[32] (Table S15 and Figure S16 in the Supporting Information). Combining the known facts, one can suppose that occurrence of five-coordinate titanium and titanyl groups in LHT-9 and its layered derivatives is related to nonperiodic structural features, namely, local truncation of octahedral Ti sites with formation of short titanyl bonds. Unexpected evidence for titanyl groups in the examined titanates was provided by analysis of their FTIR spectra (Figure 5 and Figure S10 in the Supporting Information). Besides a series of absorption bands between 800 and 400 cm^{-1} attributable to internal modes of TiO_6 octahedra, the FTIR spectra of each studied layered titanate contained a high-frequency band at 900−915 cm^{-1} that could not be ascribed to vibrations of long Ti−O bonds in TiO_6 octahedra (Figure S14 in the Supporting Information). Meanwhile, this band is very well developed in the FTIR spectrum of $K_2Ti_2O_5$ (Figure 5). Raman spectroscopy studies of $K_2Ti_2O_5$[32] and lepidocrocite-type titanates[33] revealed that this band appears in their Raman spectra as well. In the case of $K_2Ti_2O_5$, the appearance of the Raman band at 898 cm^{-1} is attributable to vibrations of the short (1.585 Å)[28] Ti═O bond in the square-pyramidal environment of titanium.[32] The same band assignments were made for Raman spectra of a series of titanosilicates containing Ti^V.[34] However, absorption bands at ∼900 cm^{-1} in the IR and Raman spectra of layered titanates have never been discussed in relation to titanyl groups. The occurrence of Ti═O groups in LHT-9 and its layered derivatives can be explained by "self-saturation" of dangling unsaturated Ti−O bonds at truncated Ti sites (Figure 11). In regard to LHT-9, it can be recalled that the crystal structure contains a significant number of vacant Ti sites (∼6%). Consequently, the local truncation of Ti sites can be associated with two different types of structural defects. The first type is related to surface defects like those reported for nanoanatase.[27] The second one implies truncation of Ti sites surrounding vacant octahedra in titanate sheets (Figure 11). The latter route can be realized only in lepidocrocite-type titanates because other layered titanate structures do not contain vacant Ti sites. If the second mechanism of formation of titanyl bonds is true, five-coordinate titanium might be considered as an inherent albeit nonperiodic structural feature of all defect-containing lepidocrocite-type titanates. Notably, the topology of an octahedral lepidocrocite sheet implies that all vacant sites are located at the surfaces of the sheets (Figures 3 and 11). Taking into account the quasi-2D nature of LHT-9 nanoleaves (Figure 2), one can suppose that titanyl groups located on the outer surfaces of the nanoleaves might significantly contribute to the overall surface activity of LHT-9.

4. CONCLUSIONS

In the present paper, we have reported on the new hybrid compound layered hydrazinium titanate (LHT-9), which bears a unique combination of chemical features: strong reductive properties, ion-exchange behavior, surface acidity, and enrichment in surface titanyl groups. LHT-9 is capable of uptake of ∼50 elements of the Periodic Table over a wide pH range, allowing its usage as an effective polyfunctional adsorbent. Thermal decomposition of LHT-9 involves intermediate stages of formation of titanium dioxide with a layered structure. The latter is supposed to be a new lepidocrocite-type polymorph of TiO_2. The new one-pot fluoride route employed for the synthesis of LHT-9 can be readily extended to the preparation of other nanocrystalline layered titanates.

■ ASSOCIATED CONTENT

Supporting Information. X-ray, structural, and FTIR data for the studied titanates and X-ray crystallographic data (CIF) for bulk LHT-9 (**2**). This material is available free of charge via the Internet at http://pubs.acs.org.

■ AUTHOR INFORMATION

Corresponding Author
sbritvin@gmail.com

■ ACKNOWLEDGMENT

L.K. gratefully acknowledges financial support by the DFG in the frame of the Heisenberg Program. This study was supported by DFG Project DE 412/39-1, Russian Federal Grant-in-Aid Contracts 02.740.11.0326 and 16.513.11.3033, an internal budget grant of St. Petersburg State University (3.37.84.2011), and DESY Proposal I-20100085.

■ REFERENCES

(1) (a) Bavykin, D. V.; Friedrich, J. M.; Walsh, F. *Adv. Mater.* **2006**, *18*, 2807–2824. (b) Chen, X.; Mao, S. S. *Chem. Rev.* **2007**, *107*, 2891–2959. (c) Sun, X.; Li, Y. *Chem.—Eur. J.* **2003**, *9*, 2229–2238. (d) Zhou, W.; Liu, H.; Boughton, R.; Du, G.; Lin, J.; Wang, J.; Liu, D. *J. Mater. Chem.* **2010**, *20*, 5993–6008.

(2) (a) Sasaki, T.; Izumi, F.; Watanabe, M. *Chem. Mater.* **1996**, *8*, 777–782. (b) Sasaki, T.; Kooli, F.; Iida, M.; Michue, Y.; Takenouchi, S.; Yajima, Y.; Izumi, F.; Chakoumakos, B. C.; Watanabe, M. *Chem. Mater.* **1998**, *10*, 4123–4128. (c) Wang, Q.; Gao, Q.; Shi, J. *Langmuir* **2004**, *20*, 10231–10237. (d) Portehault, D.; Giordano, C.; Sanchez, C.; Antonietti, M. *Chem. Mater.* **2010**, *22*, 2125–2131.

(3) Reid, A. F.; Mumme, W. G.; Wadsley, A. D. *Acta Crystallogr., Sect. B* **1968**, *24*, 1228–1233.
(4) (a) Audrieth, L. F.; Ogg, B. A. *The Chemistry of Hydrazine*; Wiley: New York, 1951. (b) Schmidt, E. W. *Hydrazine and Its Derivatives: Preparation, Properties, Applications*, 2nd ed.; Wiley: New York, 2001.
(5) (a) Mitzi, D. B.; Kosbar, L. L.; Murray, C. E.; Copel, M.; Afzali, A. *Nature* **2004**, *428*, 299–303. (b) Mitzi, D. B. *Inorg. Chem.* **2005**, *44*, 3755–3761. (c) Mitzi, D. B.; Copel, M.; Chey, S. J. *Adv. Mater.* **2005**, *17*, 1285–1289. (d) Milliron, D. J.; Mitzi, D. B.; Copel, M.; Murray, C. E. *Chem. Mater.* **2006**, *18*, 581–590. (e) Mitzi, D. B.; Copel, M.; Murray, C. E. *Adv. Mater.* **2006**, *18*, 2448–2452. (f) Mitzi, D. B. *Inorg. Chem.* **2007**, *46*, 926–931. (g) Manos, M. J.; Kanatzidis, M. G. *Inorg. Chem.* **2009**, *48*, 4658–4660.
(6) Asazawa, K.; Yamada, K.; Tanaka, H.; Oka, A.; Taniguchi, M.; Kobayashi, T. *Angew. Chem.* **2007**, *119*, 8170–8173.
(7) (a) Unal, U.; Matsumoto, Y.; Tanaka, N.; Kimura, Y.; Tamoto, N. *J. Phys Chem. B* **2003**, *107*, 12680–12689. (b) Matsumoto, Y.; Unal, U.; Kimura, Y.; Ohashi, S.; Izawa, K. *J. Phys Chem. B* **2005**, *109*, 12748–12754.
(8) Fang, K.; Kaschak, D. M.; Sutorik, A. C.; Mallouk, T. E. *J. Am. Chem. Soc.* **1997**, *119*, 12184–12191.
(9) (a) Britvin, S. N.; Siidra, O. I.; Lotnyk, A.; Krivovichev, S. V.; Depmeier, W. *Eur. J. Inorg. Chem.* **2010**, 1082–1088. (b) Britvin, S. N.; Spiridonova, D. V.; Siidra, O. I.; Lotnyk, A.; Kienle, L.; Krivovichev, S. V.; Depmeier, W. *Microporous Mesoporous Mater.* **2010**, *131*, 282–288.
(10) Britvin, S. N.; Krivovichev, S. V.; Depmeier, W.; Siidra, O. I.; Spiridonova, D. V.; Gurzhiy, V. V.; Zolotarev, A. A. PCT Pat. Appl. PCT/EP2010/001864, filed March 25, 2010.
(11) (a) Sasaki, T.; Watanabe, M.; Michiue, Y.; Komatsu, Y.; Izumi, F.; Takenouchi, S. *Chem. Mater.* **1995**, *7*, 1001–1007. (b) Matsumoto, Y.; Funatsu, A.; Matsuo, D.; Unal, U.; Ozawa, K. *J. Phys. Chem. B* **2001**, *105*, 10893–10899.
(12) Berry, K. L.; Aftandilian, V. D.; Gilbert, W. W.; Meibohm, E. P. H.; Young, H. S. *J. Inorg. Nucl. Chem.* **1960**, *14*, 231–234.
(13) Sheldrick, G. M. *SHELX-97: Programs for Crystal Structure Analysis*; University of Göttingen: Göttingen, Germany, 1997.
(14) References for FULLPROF, a program for Rietveld refinement and pattern matching analysis: (a) Rodriguez-Carvajal, J. *Abstracts of Papers*, Satellite Meeting on Powder Diffraction of the XVth Congress of the IUCr, Toulouse, France, 1990; p 127. (b) Rodriguez-Carvajal, J. *Physica B* **1993**, *192*, 55.
(15) Ravel, B.; Newville, M. *J. Synchrotron Radiat.* **2005**, *12*, 537–541.
(16) Lokshin, E. P.; Belikov, M. L. *Russ. J. Appl. Chem.* **2008**, *81*, 165–169.
(17) England, W. A.; Birkett, J. E.; Goodenough, J. B.; Wiseman, P. J. *J. Solid State Chem.* **1983**, *49*, 300–308.
(18) *Inorganic Crystal Structure Database (ICSD)*; FIZ Karlsruhe: Karlsruhe, Germany, 2011.
(19) (a) Sasaki, T.; Watanabe, M.; Hashizume, H.; Yamada, H.; Nakazawa, H. *J. Am. Chem. Soc.* **1996**, *118*, 8329–8335. (b) Sasaki, T.; Watanabe, M. *J. Phys. Chem. B* **1997**, *101*, 10159–10161. (c) Takagaki, A.; Sugisawa, M.; Lu, D.; Kondo, J. N.; Hara, M.; Domen, K.; Hayashi, S. *J. Am. Chem. Soc.* **2003**, *125*, 5479–5485. (d) Takagaki, A.; Yoshida, T.; Lu, D.; Kondo, J. N.; Hara, M.; Domen, K.; Hayashi, S. *J. Phys. Chem. B* **2004**, *108*, 11549–11555.
(20) Mezyk, S. P.; Tateishi, M.; MacFarlane, R.; Bartels, D. M. *J. Chem. Soc., Faraday Trans.* **1996**, *92*, 2541–2545.
(21) (a) Snyder, R. G.; Decius, J. C. *Spectrochim. Acta* **1959**, *13*, 280–290. (b) Schettino, V.; Salomo, R. E. *Spectrochim. Acta, Part A* **1974**, *30*, 1445–1450.
(22) (a) Goubeau, J.; Kull, U. *Z. Anorg. Allg. Chem.* **1962**, *316*, 182–189. (b) Braibanti, A.; Dallavalle, F.; Pellinghelli, M. A.; Leporati, E. *Inorg. Chem.* **1968**, *7*, 1430–1433.
(23) (a) Hervieu, M.; Raveau, B. *Rev. Chim. Miner.* **1981**, *18*, 642–649. (b) Grey, I. E.; Li, C.; Madsen, I. C.; Watts, J. A. *J. Solid State Chem.* **1987**, *66*, 7–19.
(24) Juza, R.; Heners, Z. *Z. Anorg. Allg. Chem.* **1964**, *332*, 159–172.
(25) Takagaki, A.; Lu, D.; Kondo, J. N.; Hara, M.; Hayashi, S.; Domen, K. *Chem. Mater.* **2005**, *17*, 2487–2489.
(26) Farges, F.; Brown, G. E.; Rehr, J. *Phys. Rev. B* **1997**, *56*, 1809–1819.
(27) (a) Luca, V.; Djajanti, S.; Howe, R. F. *J. Phys. Chem. B* **1998**, *102*, 10650–10657. (b) Chen, L. X.; Rajh, T.; Jäger, W.; Nedeljkovic, J.; Thurnauer, M. C. *J. Synchrotron Radiat.* **1999**, *6*, 445–447. (c) Wang, W.; Varghese, O. K.; Paulose, M.; Grimes, C. A. *J. Mater. Res.* **2004**, *19*, 417–422. (d) Saponjic, Z. V.; Dimitrijevic, N. M.; Tiede, D. M.; Goshe, A. J.; Zuo, X.; Chen, L. X.; Barnard, A. S.; Zapol, P.; Curtiss, L.; Rajh, T. *Adv. Mater.* **2005**, *17*, 965–971. (e) Flank, A.-M.; Lagarde, P.; Itié, J.-P.; Polian, A.; Hearne, G. R. *Phys. Rev. B* **2008**, *77*, No. 224112.
(28) Andersson, S.; Wadsley, A. D. *Acta Chem. Scand.* **1961**, *15*, 663–669.
(29) (a) Andersson, S.; Wadsley, A. D. *Acta Crystallogr.* **1961**, *14*, 1245–1249. (b) Verbaere, A.; Tournoux, M. *Bull. Soc. Chim. Fr.* **1973**, 1237–1241. (c) Kwiatkowska, J.; Grey, I. E.; Madsen, I. C.; Bursill, L. A. *Acta Crystallogr., Sect. B* **1987**, *43*, 258–265.
(30) (a) Cottineau, T.; Richard-Plouet, M.; Rouet, A.; Puzenat, E.; Sutrisno, H.; Piffard, Y.; Petit, P.-E.; Brohan, L. *Chem. Mater.* **2008**, *20*, 1421–1430. (b) Nakahira, A.; Kubo, T.; Numako, C. *Inorg. Chem.* **2010**, *49*, 5845–5852.
(31) (a) Ma, R.; Fukuda, K.; Sasaki, T.; Osada, M.; Bando, Y. *J. Phys. Chem. B* **2005**, *109*, 6210–6214. (b) Kubo, T.; Honma, T.; Umesaki, M.; Nakahira, A. *J. Soc. Mater. Sci. Jpn.* **2006**, *55*, 666–669.
(32) Bamberger, C. E.; Begun, G. M.; MacDougal, C. S. *Appl. Spectrosc.* **1990**, *44*, 30–37.
(33) Peng, C.-W.; Richard-Plouet, M.; Ke, T.-Y.; Lee, C.-Y.; Chiu, H.-T.; Marhic, C.; Puzenat, E.; Lemoigno, F.; Brohan, L. *Chem. Mater.* **2008**, *20*, 7228–7236.
(34) Su, Y.; Balmer, M. L.; Bunker, B. C. *J. Phys. Chem. B* **2000**, *104*, 8160–8169.